Two-Dimensional Layers of Colloidal CdTe Quantum Dots: Assembly, Optical Properties, and Vibroelectronic Coupling

Thomas Noblet, Souhir Boujday, Christophe Methivier, Marie Erard, Julie Hottechamps, Bertrand Busson, Christophe Humbert

2D-Layers of Colloidal Quantum Dots: Assembly, Optical Properties and Vibroelectronic Coupling

T. Noblet,*[a][c] S. Boujday,[b] C. Méthivier,[b] M. Erard,[a] J. Hottechamps,[c] B. Busson [a] and C. Humbert[a]

Abstract: The manufacturing of silica platforms functionalized by CdTe quantum dots (QDs) of 3.4 nm diameter through (3-aminopropy)triethoxysilane (APTES) aliphatic organosilanes is performed to preserve QDs excitonic properties after their transfer from colloidal solutions to surfaces at ambient air. In these conditions, the chemical stability and the structural homogeneity of monolayers are monitored and attested by probing their optical efficiency through UV-Visible spectroscopy (absorption), time-resolved fluorescence spectroscopy and microscopy (emission). The grafting of the aliphatic organosilanes on silicon is examined by XPS measurements that show that a 0.9 nm sublayer thickness is electrostatically stabilized between SiO_2 substrates and QDs layers without EDC-NHS (1-ethyl-3-(3-dimethyl-aminopropyl)carbodiimide, N-hydroxysuccinimide) activation. Surprisingly, in the latter case, the optical absorption of the QD layer does not vary beyond 10 days while it degrades in one day if QDs are activated. Finally, SFG spectroscopy evidences a vibroelectronic coupling between the QDs and APTES monolayers constituting the platforms.

Introduction

In surface chemistry, many research groups are specialized in the chemical functionalization of interfaces, with the aim of developing biosensors [1,2], molecular recognition devices [3] or heterogeneous catalysts [4]. The design of such interfaces often results in the preparation of monolayers, composed of both molecules and nanoparticles [5,6]. These interfaces have several advantages: unlike the deposition protocols based on spin-coating or drop-casting, the assembly of monolayers leads to homogeneous samples with a good reproducibility, and is relatively economical in terms of raw materials. The various works carried out on gold nanoparticles clearly testify to this [5,7–9], by evidencing that the homogeneity of the grafting and the good dispersion of the nanoparticles are crucial: if the nanoparticles aggregate on the substrate during their deposition, their optical properties (ie. plasmonics) are dramatically altered, making them difficult to operate for the design of chemical sensors. In the case of semiconductor quantum dots (QDs), this chemical approach through self-assembled monolayers is not as much popular. The literature indeed counts very few attempts [10]. Instead, the community favors evaporation-induced self-assembly [11,12], drop-casting [13], template-patterning [14,15] and Langmuir-Blodgett deposition [16]. In this article, we aim at the implementation of QD deposition thanks to surface chemistry (at ambient working conditions) and do want to prove this is of high interest for the design of QD-based functional platforms.

[a] Dr. T. Noblet, Prof. M. Erard, Dr. B. Busson, Dr. C. Humbert
Université Paris-Saclay, CNRS, Institut de Chimie Physique, UMR 8000, 91405, Orsay, France
[b] Prof. S. Boujday, Dr. C. Méthivier
Sorbonne Universités, UPMC Univ. Paris 6, UMR CNRS 7197
Laboratoire de Réactivité de Surface, F75005 Paris, France
[c] Dr. T. Noblet (current address), J. Hottechamps
GRASP-Biophotonics, CESAM, University of Liège, Institute of Physics, Allée du 6 août 17, 4000 Liège, Belgium
E-mail: t.noblet@uliege.be

Supporting information for this article is given via a link at the end of the document.

First, we show how to transfer COOH-conjugated CdTe QDs from colloidal aqueous solutions to solid silica substrates (glass and silicon) without denaturing their excitonic properties: the absorption and emission spectra do not undergo any spectral shift, contrary to what has already been observed for Langmuir-Blodgett deposits of PbS/PbSe QDs [16]. The CdTe QDs we use are capped with mercaptopropionic acids [21] and characterized by a mean diameter of 3.4 nm [31]. In order to immobilize them and achieve 2D-monolayers, we use amine-terminated aliphatic organosilanes (3-aminopropy)triethoxysilane (APTES) as grafting chemical agents, given their ability to bind with silica surfaces (SiO_2) by heterocondensation with silanol moieties [5,17-20]. X-ray Photoelectron Spectroscopy (XPS) is performed to characterize the thickness and the coverage rate of APTES and to approve the good quality of the self-assembled underlayer. Since then, the amine terminals of APTES enable the QDs to attach to the platform, *via* electrostatic interactions or covalent bonds. These two strategies are investigated and compared. Our results henceforth evidence that the electrostatic interactions between APTES (NH_3^+) and QD ligands (COO^-) is by far the most stable chemical configuration with respect to covalent bonds. This counterintuitive result is stated on comparative optical measurements based on UV-Visible absorption spectroscopy and supported by time-resolved fluorescence measurements. As a matter of fact, our method leads to QD monolayers which are dense, homogeneous, stable, reproducible and strongly coupled to APTES. In addition, we use nonlinear optical Sum-Frequency Generation (SFG) spectroscopy to assess the range and the strength of the coupling between QDs and APTES. Indeed, QDs are known to couple with their molecular environment through dipolar interaction [21]. Here, SFG spectroscopy validates the existence of such a coupling and evidences that the electronic structure of the grafted QDs interacts with the vibrational structure of APTES. These results open the door to the soft, easy and cheap design of robust and optically functional QD-based platforms dedicated to chemical and biological sensing. This is all the more promising than we here succeed in handling 3 nm size particles, touching on the lower limit of nanoscale.

Results and Discussion

Assembly of QD monolayers

The chemical protocol to build CdTe QD-based silica (silicon or glass) platforms is depicted in Figure 1 and detailed in the Experimental section. Two strategies can be considered for immobilizing QDs onto silica substrates silanized by APTES. The bonds which are established between the carboxylic ligands of QDs and the amine functions of APTES can be electrostatic/ionic (Figure 1d) or covalent (Figure 1e). In the first case (physisorption strategy), we bathe the silanized substrates in a colloidal solution of QDs and let them assemble while, in the second case (chemisorption strategy), a preliminary activation step is mandatory. Indeed, the carboxylic functions of the ligands cannot effectively bind spontaneously to amine functions [22]. The formation of amide bonds requires the use of activators [23–25], such as: EDC, ie. 1-ethyl-3-(3-dimethylaminopropyl)carbodiimide, and NHS, ie. N-hydroxysuccinimide, both depicted in Figure 1f. In particular, the question is to determine whether the physi- or the

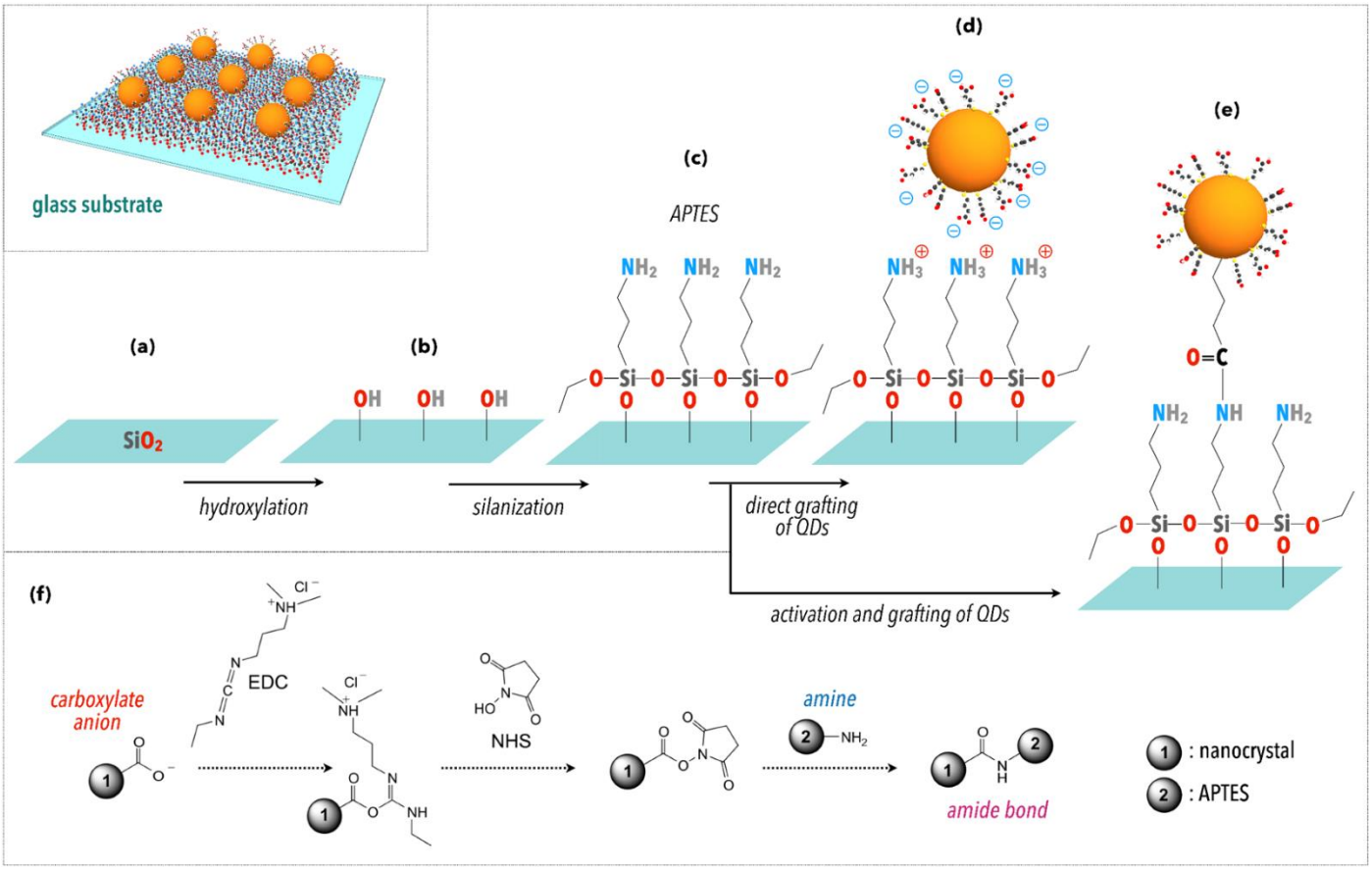

Figure 1. Global description of the different steps of the protocol leading to the deposition of a QD monolayer on a silica substrate (borosilicate glass slide or wafer of intrinsic silicon). **(a)** The substrate initially has a surface layer of SiO_2 oxide. **(b)** Hydroxylation then leads to the activation of silanol groups which serve as **(c)** the attachment base for the APTES molecules. The grafting of the QDs can therefore be obtained by **(d)** electrostatic affinity between the carboxylates on the surface of nanocrystals and the amine terminations of the APTES (ionic bonds) or **(e)** by catalyzing the formation of amide bonds between these same groups (covalent bonds).

chemisorption strategies are the most relevant for the immobilization of QDs, from the point of view of their chemical stability. In the next sections, we indeed characterize and compare the efficiencies of these two strategies.

Chemical characterization of APTES underlayer

In order to get an idea of the density of APTES molecules that we graft on the substrates (Figure 1c), we analyze a silanized silicon wafer (Si-APTES) by XPS in Figure 2. The results discussed hereafter come from calculations detailed in Supporting Information (section I). The XPS spectra of Figure 2 highlight the presence of 1.7 molecules of APTES per nm^2. To achieve this surface density, two intermediate quantities must be determined: the thickness of the oxide, d_{SiO2}, covering the silicon substrate and the thickness of the APTES layer, d_{APTES}. The first one is derived from the measurements of the intensities I_{SiO2} and I_{Si} associated to the Si:2p XPS peaks coming from the Si elements of the oxide layer and the substrate, respectively. This gives $d_{SiO2} = 1$ nm. The second thickness is calculated from Beer-Lambert's law: by measuring the attenuation of the XPS signal associated with the substrate (I_{Si}, Si:2p electronic state) and the intensity of the carbon XPS peak of APTES (I_{APTES}, C:1s electronic state), it is possible to deduce $d_{APTES} = 0.9$ nm. With these two values and by measuring the XPS signal linked to the nitrogen of the amine functions (I_{APTES}, N:1s electronic state), we can calculate $N_{APTES} = 1.7$ nm^{-2}. Besides, the XPS spectrum of the N:1s electronic state confirms the presence of NH_3^+ protonated groups on the surface, and therefore supports the possibility of an electrostatic stabilization of the APTES monolayer. Indeed, SiO_2 surfaces tend to charge negatively [26], which promotes, or at least stabilizes, the protonation of the amines of APTES into NH_3^+.

In the following, we choose to work on a glass substrate because the spectroscopic characterizations by UV-visible are much more sensitive when we probe the samples by transmission, whereas silicon wafers can only be probed in reflection.

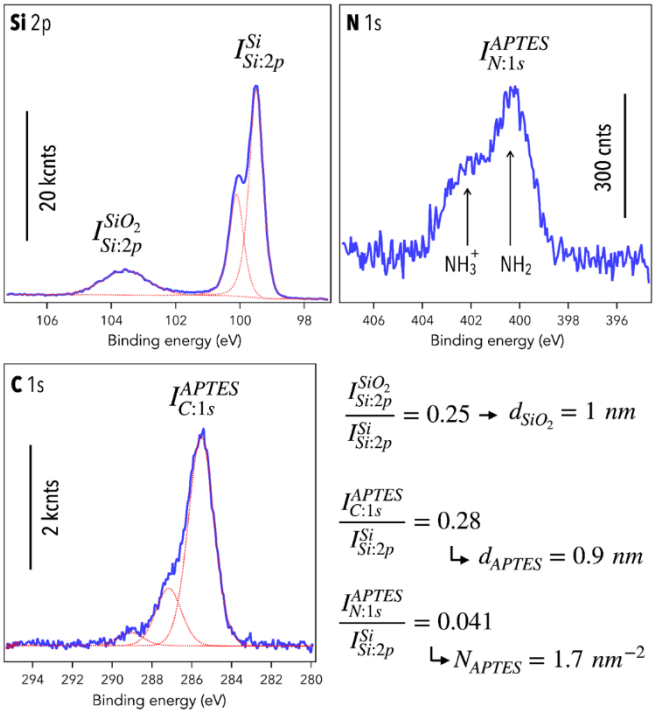

Figure 2. Summary of the XPS analysis carried out for a silicon substrate Si(100) covered by APTES. This analysis is based on the XPS spectra related to silicon (Si:2p state), carbon (C:1s state) and nitrogen (N:1s state) as detailed in the text and in Supporting Information (section I).

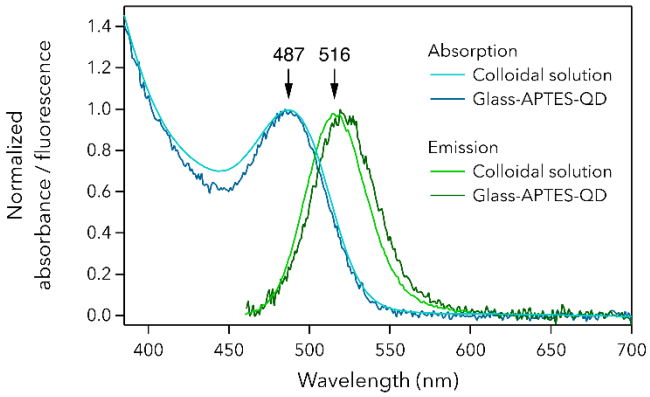

Figure 3. Comparison of the absorption and emission optical properties of Glass-APTES-QD samples with respect to the reference colloidal solution.

Optical characterization of physisorbed QD monolayers

We first consider the case of QD monolayers obtained by physisorption on silanized glass (Figure 1d). Since the pKa of amines is around 10 [27], we expect the protonated form of APTES to be predominant in the aqueous medium, when the silanized substrates are immersed in the colloidal solution of QDs (pH 5.5). As the surface of COOH-conjugated CdTe QDs is negatively charged (their zeta potential is -36 mV [28]), there exist significant attractive ionic forces between the carboxylates of the QDs and the terminal NH_3^+ of APTES (Figure 1d). As observed on Figure 3, such a Glass-APTES-QD sample presents the same optical properties that the colloidal QDs solution. The local maximum of absorption is located at 487 nm in both cases. For the fluorescence emission, a very slight redshift of the emission band from 516 nm to 522 nm is observed (6 nm). It is quite smaller than that observed for Langmuir–Blodgett monolayers of PbS QDs [22]. Interestingly, the adsorption of QDs does not convey into any spectral broadening, which means that the statistical distribution of QD sizes on silica is very close to that of the colloidal solution. With respect to the absorption spectra, the distribution even seems pretty narrower in the case of QD monolayers. Thereby, these spectra prove the very good grafting quality of the QDs in the presence of an underlayer of APTES.

Density and stability of physi- and chemisorbed QD monolayers

As suggested by the literature [29,30], the grafting of COOH-coated nanoparticles to an amine-functionalized surface is expected to be stabilized thanks to the use of EDC and NHS, as activators of the formation of amide bonds. This is why we chose to investigate this chemisorption strategy and to compare it with physisorption.

In order to operate this comparison between the adsorption made with and without EDC-NHS activation, we can first determine the QDs surface densities. For this, we measure the absorbance of Glass-APTES-QD samples (without activation) and Glass-APTES-QD* samples (with activation) prepared simultaneously under the same conditions. The results are shown in Figure 4a. At first glance, the two types of samples do not reveal any major difference. We clearly distinguish the local maximum absorbance of the QDs at 487 nm, and the spectra are characterized by comparable intensity levels and similar shapes. Thanks to the modeling of the UV-visible spectra that we developed in a previous work for colloidal solutions [21], here applied to the case of monolayers (see Supporting Information, section II), it is possible to extract from these measurements the surface coverages of the QDs. The fits reported in Figure 4a give us a density N_s = 5.4 10^{-2} nm^{-2} for Glass-APTES-QD, and N_s^* =

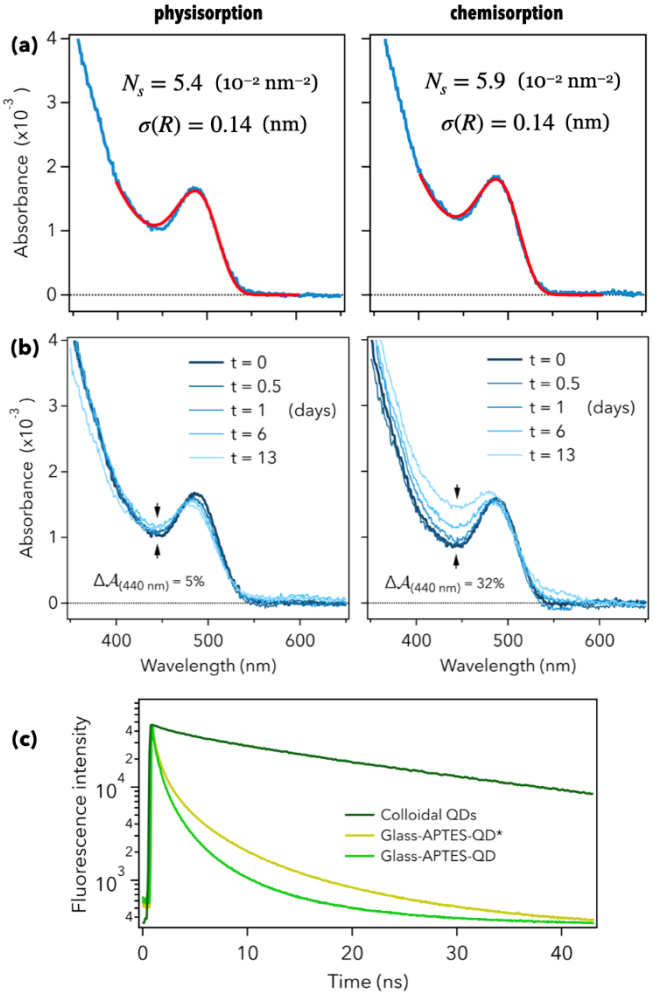

Figure 4. (a) UV-visible spectra of Glass-APTES-QD samples obtained without activation of QDs (left column) and of Glass-APTES-QD* samples obtained with activation of QDs by EDC-NHS (right column). The red curves are fits to the experimental data (see Supporting Information, section II). Here, the surface density N_s of QDs and their radius dispersion $\sigma(R)$ are the fitting parameters. **(b)** Kinetic study of the UV-visible extinction spectra of non-activated (left) and activated (right) samples. The time t = 0 corresponds to the time after the samples are taken out of their QD baths, rinsed and dried. For each sample, we calculate ΔA_{440nm} as explained in the text and detailed in Supporting Information (section II, Fig. C). **(c)** Time-resolved measurements of the fluorescence emitted by CdTe QDs in colloidal solution and in monolayers, both on Glass-APTES-QD and Glass-APTES-QD* samples (for t = 0).

5.9 10^{-2} nm^{-2} for Glass-APTES-QD*. The values are equivalent for both protocols and translate into a surface coverage of 45%. The other samples shown in Supporting Information (section II, Fig. B and C) give the same results and thus validate the reproducibility of the two methods of deposition. Given the surface density of APTES, N_{APTES} = 1.7 nm^{-2}, previously determined by XPS, we deduce that each QD has a grafting base of around 35 APTES molecules, which seems reasonable for obtaining chemically stable deposits over time. Assuming an ideal QD monolayer, the average distance between QDs can be estimated by $1/\sqrt{N_s}$, which in both cases leads to a value around 4.5 nm, indeed greater than the diameter of the QDs (3.4 nm). Consequently, our measurements have been so far compatible with the hypothesis of a monolayer and have validated the accuracy of the two protocols in terms of coverage rate, reproducibility and optical properties.

The stability is meanwhile tested for each sample by acquiring time-delayed UV-visible spectra. Figure 4b gathers the spectra acquired for five different storage times. It is worth noting that all the samples were stored in individual plastic boxes in a fume hood at 20°C, just after their preparation and between measurements, to avoid any chemical contamination. In this way, the durability of the monolayers is tested over a maximum of 13 days. The deposits obtained by chemisorption are clearly less stable than

those simply obtained by physisorption. We notice that scattering gradually appears for Glass-APTES-QD* samples, from the first day: the associated UV-visible spectra exhibit an increase in extinction on either side of the first absorption peak. This phenomenon is similar to that observed and explained in colloidal solutions in a recent work [28]. Conversely, the shape of the spectra of Glass-APTES-QD samples remains unchanged over the same 13 days. We thus conclude that the samples obtained by chemisorption are subject to an aggregation of QDs, even once grafted on the substrate. The action of the EDC-NHS couple as it was observed and described in [28] apply here even though CdTe QDs are transferred on a silanized substrate. To quantify this effect, we calculate for each sample the standard deviation ΔA_{440nm} of the absorbance at 440 nm, as defined and detailed in Supporting Information (section II): it is expressed as a percentage of the initial value A_{440nm} (t = 0). If we are interested in the values taken by the absorbance of the samples at 440 nm, this is due to the fact that the scattering, whose cross-section is governed by $\sigma_d(\lambda) \sim \lambda^{-4}$, is more effective at small wavelengths, and that it manifests itself critically at the local minimum of the spectra presented in Figure 4b, between 440 and 450 nm. The calculations reported in the figure, and in Supporting Information (section II, Fig. C) for additional samples, then show that this standard deviation clearly discriminates the two protocols. It varies between 15 and 40% for Glass-APTES-QD*, against only 5 to 7% for Glass-APTES-QD. According to this quantitative criterion, the non-activated samples are the most stable by far, with equivalent QDs surface densities for both protocols.

Contrary to what we could believe, the deposition protocol based on physisorption must be preferred over that which targets a fixation by chemisorption. From our point of view, it would be related to the following reasons: I) Without activation, the QDs keep their negative charges on the surface, the ligands mainly remaining deprotonated (COO^-), which ensures electrostatic repulsion between QDs and prevents them from a possible agglomeration; II) When QDs are activated, only a small part of the APTES molecules actually binds to the ligands to form amide bonds. This would mean that there are more electrostatic interactions between QDs and APTES in the case of physisorption than covalent bonds in the case of chemisorption. To support this hypothesis, we measure the fluorescence decays of QDs grafted on glass using a fluorescence lifetime imaging setup (Figure 4c). Both decays are compared with that of the colloidal solution wherein the QDs are free, isolated and not coupled with their environment. The average decay time of the colloidal QDs is estimated at 24 ns (computed in Supporting Information, section III). The deposition of the QDs on silanized substrates leads to a strong decrease of their average fluorescence lifetime (to 1.0 ns for physisorption and 1.6 ns for chemisorption) and thus to an efficient fluorescence quenching most likely due to couplings between the emitters and their environment. Besides, we observe that the Glass-APTES-QD sample exhibits a fluorescence decay significantly shorter than that recorded for the Glass-APTES-QD* one. This can be due to the fact that the physisorbed QDs establish more interactions with their environment than the chemisorbed QDs. In summary, the arising of shorter fluorescence times for the samples obtained without EDC-NHS confirms that the QDs grafted without activation are more coupled to APTES than those deposited through activation. In the following, we therefore only work with physisorbed QDs.

Spatial homogeneity of physisorbed QD monolayers

Given the small size of the QDs we are studying (3.4 nm), it is not possible to see them by optical imaging but thanks to electron microscopy. However, HR-TEM does not allow to study deposits on glass or silicon substrates: the QDs must be deposited on

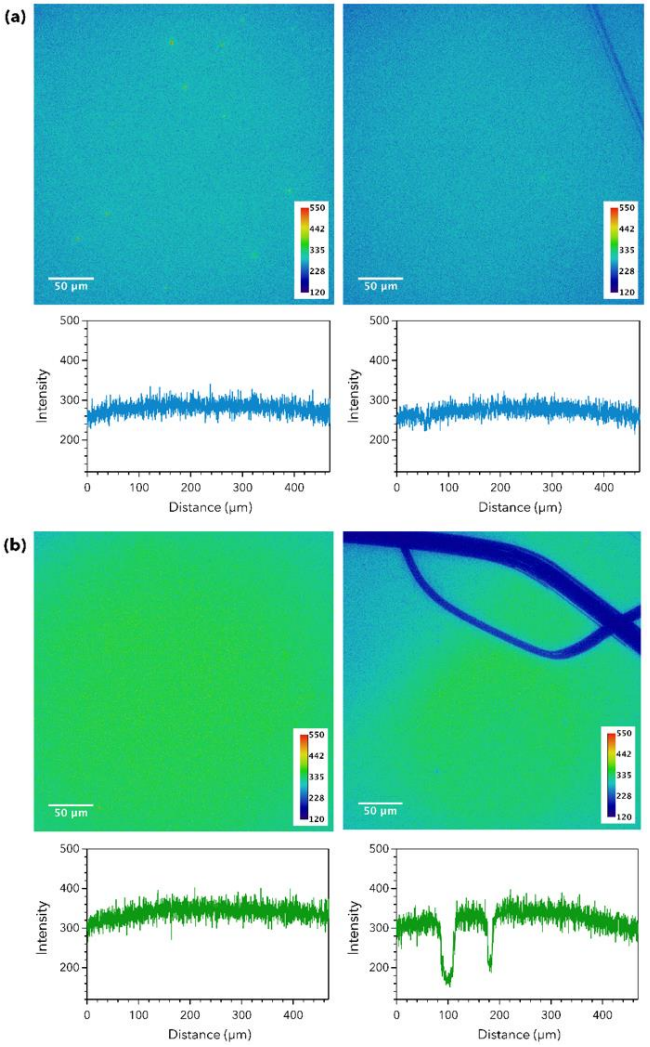

Figure 5. Fluorescence images and intensity profile plots along the anti-diagonal of two independent sample of QDs monolayers on glass (Glass-APTES-QD) **(a)** and **(b)**. For each sample, we display fluorescence images of two regions of interest away from 1 cm (left and right). The black color of the intensity color scale corresponds to the background in absence of QDs. It is at an intensity level of 120. The black scratches on picture **(b)** at right, are intentional, in order to attest the presence of QDs in the fluorescent pixels.

metal grids [31]. This is why we used UV-visible spectroscopy to calculate the surface coverage N_S, hence the importance of the operational analytical model we previously developed to extract N_s from absorption spectra [21]. To assess the uniformity of the QD layer, we face the same difficulties: direct optical and electronic microscopies do not allow to image monolayers. Nevertheless, we took advantage of the fluorescence of the QDs to characterize the uniformity of the monolayers by directly taking fluorescence images of the samples thanks to optical fluorescence microscopy (Figure 5).

For the two Glass-APTES-QD surfaces, the pictures and the profiles exhibit constant levels of fluorescence intensity: on the one hand, at the scale of each image (ie. 500 µm along the diagonal), and on the other hand, from one point of the sample to another (the two regions of interest of each sample are 1 cm away). It is worth noting that the above pictures cover an area of 333x333 µm², which corresponds to a number of 6,5 10^9 QDs. This characterization therefore tells us that the spatial distribution of QDs in the monolayers are very homogeneous, although we can guess a few hot spots in Figure 5a. These results *a fortiori* prove that the APTES underlayer is itself homogeneous and demonstrate the relevance of the entire protocol. Now that we are in possession of high-quality samples, we must examine how the electronic response of the QDs is coupled to the vibration modes

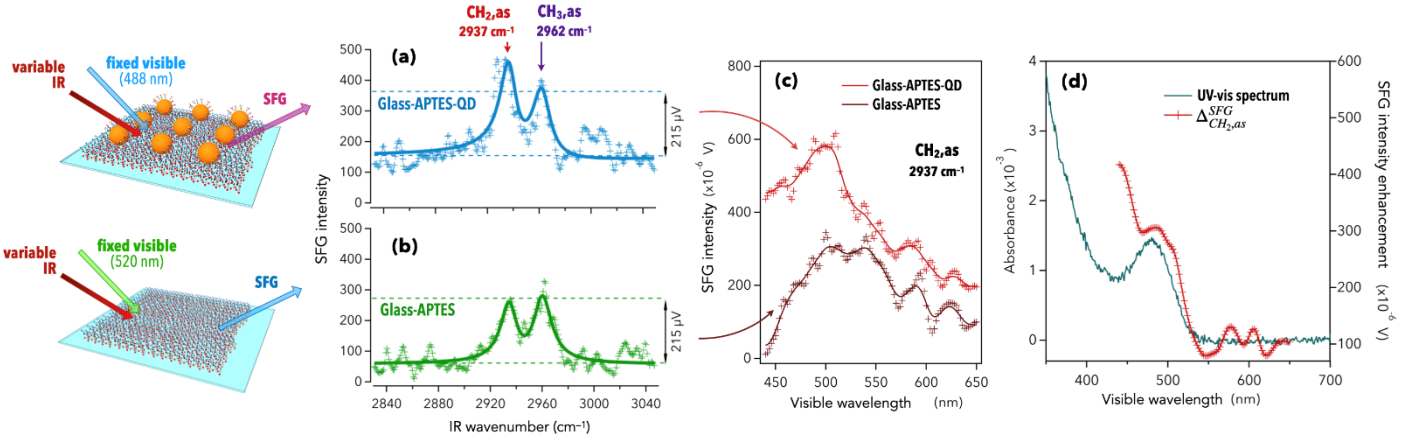

Figure 6. Vibrational SFG spectra of **(a)** Glass-APTES-QD (in blue) and **(b)** Glass-APTES (in green), respectively obtained for visible wavelengths of 520 nm and 487 nm for [s:sp] polarizations scheme. The solid lines correspond to the fitting procedure detailed in Supporting Information (section IV) based on [21], taking into account two vibrations. **(c)** Electronic SFG spectra (at variable visible wavelength) of the samples of **(a)** and **(b)**, obtained for an IR wavenumber set at 2937 cm^{-1} corresponding to the asymmetric stretching vibration mode of the methylene (CH_2, as) chemical group of APTES. The continuous curves are averages. **(d)** Superposition of the UV-visible spectrum of Glass-APTES-QD and the quantity $\Delta_{CH2\ as}^{SFG}$ defined in the text as the subtraction of the two spectra of figure **(c)**.

of APTES. The characterization of such an interaction will teach us about the optical functionality of our platforms for biosensing.

Vibroelectronic coupling between QDs and APTES

In order to assess the range of an optoelectronic coupling between QDs and APTES, we use nonlinear optical SFG spectroscopy. This experimental tool allows demonstrating the existence of a vibroelectronic coupling at QD/molecule interfaces: a dipolar coupling from QDs excitons to their ligands vibrations was recently evidenced [21]. This requires the unconventional configuration of two-color SFG spectroscopy (2C-SFG). It indeed combines two visible and infrared laser excitations, continuously tunable in frequency, to simultaneously probe the electronic and the vibrational responses of the samples [32]. So far, some research works have evidenced the relevance of 2C-SFG spectroscopy for the study of structured interfaces on a molecular scale or at nanoscale, with the aim of characterizing intramolecular vibronic couplings [33,34], substrate/molecules interactions [35–39] or nanostructures/molecules interactions [40–45]. Nevertheless, the last case remains largely unexplored [44]. To date, only metallic gold nanostructures have been studied, in particular from the point of view of their plasmonic properties. In the cases of gold nanoparticle monolayers on silicon substrates [7] or gold nano-pillars synthesized on metallic substrates (Au, Pt) [42], functionalized in both cases by alkanethiols, 2C-SFG demonstrates the existence of a coupling between gold plasmons and molecular vibrations: the vibrational response of organic molecules is in fact amplified by the excitation of the localized surface plasmon characteristic of these nanostructures [41,46,47]. Our work naturally falls within this latter category, and even attempts to broaden the framework of the study of nanostructure/molecule interactions by 2C-SFG spectroscopy in the case of semiconductor nanomaterials.

To do so, we investigate and compare two samples: Glass-APTES and Glass-APTES-QD (Figure 6). The glass substrate alone does not show any significant specific SFG response. It only contributes to a weak non-resonant background over the probed infrared spectral range. The SFG spectrum of Figure 6b (Glass-APTES) supports that point. It provides the vibrational description of the Glass-APTES interface over the 2840-3040 cm^{-1} IR spectral range. As we intend to discriminate the influence of QDs on APTES, the SFG signal of this simply silanized sample thus constitutes our reference spectrum: it exhibits a very low level of molecular signal (300 µV maximum), whereas we ideally work with signals from a few units to a few tens of millivolts [45]. We therefore understand the experimental challenge that arises to succeed in demonstrating a QD/molecule coupling within interfaces producing such a weak signal SFG. The non-resonant background is 50 µV (lower dotted line) and dominated by the resonant molecular response of 300 µV. The fitting of this spectrum (see Supporting Information, section IV) reveals two resonances: the first one, at 2937 cm^{-1}, can be attributed to the asymmetric C-H elongation mode of the methylene -(CH_2)- present in the APTES alkane chain [7] (Figure 1c); and the second one, at 2962 cm^{-1}, can be assigned to the asymmetric C-H elongation mode of methyl groups -CH_3 [7]. *A priori*, the self-assembled APTES monolayer does not exhibit any methyl termination if the silanization is accompanied by a complete hydrolysis of the ethoxy groups which do not participate in the heterocondensation. However, the literature shows that these ethoxy reacts only partially, and leads to think that terminal -CH_3 are present in the resulting APTES monolayer [7,48–50] (Figure 1c). The location of the vibrations modes in Figure 6b is moreover similar to what has been previously observed on analogous silanized silicon wafers [7]. This confirms that the spectrum is here characteristic of the APTES monolayer.

To show the effect of QDs on the APTES vibrational signal, we acquire the SFG spectrum presented in Figure 6a for a Glass-APTES-QD sample. The associated UV-visible spectrum is given in Figure 6d, attesting to a good deposition of the QDs. On the SFG spectrum, we first notice an overall enhancement of the intensity level of one hundred µvolts, resulting in a non-resonant background of 150 µV (lower dotted line). In addition, this overall increase in SFG intensity comes with a more specific growth of the signal associated with the vibration mode of -(CH2)- at 2937 cm^{-1}. At first glance, this gain in intensity for methylenes could be due to the presence of the carboxylic ligands of QDs, which themselves have -(CH_2)- in their alkane chains. However, assuming QDs have a spherical geometry, the orientational distribution of their ligands follows a centrosymmetry which leads to a negligible contribution, according to the symmetry rules of the SFG process. Furthermore, as observed in a previous work [21], the vibrational signal SFG of the mercaptocarboxylic ligands is not only characterized by the asymmetric stretching mode of methylenes, but also by two additional stretching modes around 2860 and 2915 cm^{-1} [21,51], which do not appear here. In other words, the vibrational signal observed on Glass-APTES-QD is once again that of APTES. We conclude that the QDs slightly amplify the response of the APTES methylene groups at 2937 cm^{-1}. This does not happen for the methyl groups (at 2962 cm^{-1}) because: I) The number of methyls is expected to be largely smaller than that of methylenes; II) The CH_2 of the APTES alkane chains are much closer to the overlying QDs than the CH_3 end-groups, which are themselves closer to the substrate (Figure 1d).

In order to further examine this apparent coupling between the QDs and the APTES methylene groups, we specifically excite the sample at the IR frequency of the associated vibration mode, 2937 cm^{-1}, and vary the wavelength of the visible excitation from 440 to 650 nm (Figure 6c). Figure 6b gives the spectra corresponding to the two previous Glass-APTES and Glass-APTES-QD samples. The SFG intensity $I_0(\lambda_{vis})$ of the reference sample (Glass-APTES) changes significantly with respect to the visible wavelength. Since APTES is not active on the visible range, this dependence of $I_0(\lambda_{vis})$ is due to the characteristics of our visible optical parametric oscillator which does not deliver a constant power over the probed spectral range (see Supporting Information, section V). If we then compare this spectrum to that of the Glass-APTES-QD sample, we note that the intensity $I_{QD}(\lambda_{vis})$ of the latter does not follow the same wavelength dependence. From 550 to 650 nm, the shape of the two spectra is the same: only an additional non-resonant contribution of one hundred millivolts is observed. From 450 to 550 nm, we observe an increase in the SFG signal in the presence of the QDs. This increase, defined by $\Delta_{CH2\ as}^{SFG} = I_{QD}(\lambda_{vis}) - I_0(\lambda_{vis})$, is plotted in Figure 6d as a function of the visible wavelength. By superimposing it on the UV-visible spectrum of the Glass-APTES-QD sample, we can see that $\Delta_{CH2\ as}^{SFG}$ is flat over the range 550-650 nm (it coincides with the increase of 100 µV assigned to the non-resonant contribution), and increases by 200 µV between 550 and 500 nm, where the QDs are just beginning to absorb. We know that the location of this absorption band corresponds to the first QDs excitonic state. As a matter of fact, $\Delta_{CH2\ as}^{SFG}$ proves to be correlated with the excitonic properties of QDs. This observation agrees with a previous study which evidenced such a correlation between the QDs and their ligands. Here, the design of QD monolayers with an underlayer of APTES enables us to extend the range of the QD/molecule interactions: in the present article, we succeed in coupling the QDs with APTES alkane chains, instead of their ligands. It means that a fine monitoring of the chemical deposition of QDs can lead to nanostructured functional platforms in which the exciton/vibration interaction is strong enough to slightly enhance the vibrational signature of the indirect molecular environment of QDs. This correlation is spatial: only the methylene of the APTES, which are close enough, are coupled to the QDs; and spectral: this coupling appears when the electronic properties of QDs are stimulated by visible light, for $\lambda_{vis} \leq 525$ nm.

Conclusions

In summary, the observation of a QD/molecule coupling between a monolayer of QDs and a monolayer of organosilane, both immobilized on silica, has been evidenced for the first time. This must be understood in conjunction with the QD/ligand coupling previously observed and interpreted as a dipolar interaction [21]. In both cases, the vibroelectronic coupling can be seen as a FRET-like interaction (Förster Resonace Energy Transfer). The specificity of FRET for the design of chemical sensors comes from the spatial selectivity of the underlying dipolar coupling: only the fluorescent species which are close enough to the QDs can interact and benefit from an energy transfer from the nanocrystals. Our observations suggest that the same spatial selectivity can be expected and exploited for the vibroelectronic coupling of the QDs with their surrounding molecules. Further, 2C-SFG enables to trigger an energy transfer from QD excitons to molecule vibrations, thus correlating two distinct optical ranges (visible and IR), while FRET requires a spectral overlap between the two protagonists. Here is a new approach for the design of biosensors combining spatial selectivity and vibrational spectroscopy.

From a chemical point of view, such platforms do not require covalent bonds between the QDs and the organic layer. The ionic bonds obtained through a simple standard chemical protocol, without the use of any catalyst or crosslinker, have led to reliable and robust QD-based platforms: QD monolayers are dense, homogeneous, stable, reproducible, strongly coupled to APTES, and exhibit the same optical functionalities than colloids. Thanks to the expertise of chemists and physicists, a wide variety of binary and ternary semiconductor alloys are available for the synthesis of QDs. In a near future, different types of QDs should be tested to optimize the working conditions by comparing the different materials and determining those which lead to the most efficient QD/molecule coupling.

Experimental Section

Chemical design of CdTe QDs monolayers on silica surfaces

For the assembly of monolayers, the protocols we use are based on wet chemistry as established in previous works on gold nanoparticles [5,7]. We present here an adaptation to the case of QDs. The process mainly consists of three steps: the first is the cleaning of the substrates from any impurity; the second is the deposit of a monolayer of APTES molecules on the substrate to build an organic sublayer favoring QDs grafting; and the third in the deposit of a QDs monolayer by immersing the silanized substrates in a colloidal solution of QDs. Figure 1 depicts the sketch of the chemical protocol. All chemicals are purchased from Sigma-Aldrich except other mention. The glass substrates used for linear and nonlinear optical spectroscopy are from VWR (ref. 631-1551 Microscope slides, borosilicate glass). The silicon substrate used for XPS characterisation is from Sil'Tronix Silicon Technologies (intrinsic silicon, 3" wafers, (100) orientation, 355-405 µm thickness). ***Substrate hydroxylation***: we start by removing the mineral and organic contaminants adsorbed on the glass or the silicon substrate by successive 5-minute ultrasonic baths in acetone (99,8%) and ethanol (99,8%). It is followed by abundant rinsing in ultrapure water (Millipore, 18 MΩ · cm) and drying under nitrogen flow (Air Liquide: 1066 Compressed nitrogen, ALPHAGAZ 1, 200 bar, L50). The dry substrates are then immersed in a "piranha" solution (caution: piranha is corrosive and must be handled with care), composed of hydrogen peroxide (H_2O_2, 60%) for one third, and sulfuric acid (H_2SO_4, 98%) for two thirds. This step allows the elimination of the last organic pollutants by hydrolysis, and facilitates the hydroxylation of the surface, obtained by immersing and rinsing the substrates in ultrapure water. As shown in Figure 1b, this step leads to the activation of Si-OH silanol groups on the surface [52–54]. The hydroxylated samples are therefore dried under nitrogen flow. ***Substrate silanization***: for this purpose, we first prepare a 5% solution of (3-aminopropyl)triethoxysilane (APTES, A3648-100ML, 98%) in anhydrous methanol (VWR, MeOH, 99,9%). 1% solution is equivalent to 1 g of APTES in 100 mL of methanol. The substrates are immersed in 4 mL of this solution for 1h30, under a fume hood at 20°C, then rinsed in methanol under sonication (4 baths of 1 min) and finally dried under nitrogen flow. The result of this process is shown in Figure 1c. ***Monolayer deposition of QDs on glass substrates***: as highlighted in Figures 1d and 1e, respectively, two chemical grafting strategies of the QDs (777935-25MG, CdTe core-type quantum dots, COOH functionalized, fluorescence at λ = 520 nm, powder) are considered. (I) For electrostatic bonding, the silanized glass substrates are simply immersed in an aqueous colloidal 4 mL solution of QDs (C = 5.10^{-7}M) for 2h, then rinsed in ultrapure water and dried under nitrogen flow. (II) For covalent bonding, the same above-mentioned 4 mL colloidal solution of QDs is prepared. In order to activate the QDs (Figure 1f), EDC and NHS are added with a QD/(EDC,NHS) ratio of 1/400. EDC-NHS are provided by GE Life Healthcare: BR100050 Amine Coupling Kit, 750 mg 1-ethyl-3-(3-dimethylaminopropyl) carbodiimide hydrochloride (EDC), 115 mg N-hydroxysuccinimide (NHS). The substrates are then immersed in the resulting solution for 2h, rinsed in ultrapure water and dried under nitrogen flow. For both protocols, all samples are kept in individual plastic boxes in a fume hood at 20°C until their use.

UV-Visible absorption spectroscopy

The UV-visible absorption spectra are acquired using a Cary-5000 spectrophotometer (Agilent). For QDs colloidal solutions, we use PMMA cuvettes of 10 mm length and 5 mm width and measure their absorbance in transmission. A first reference measurement is made with the solvent alone (ultrapure water). The QDs spectra are therefore obtained by subtracting the absorbance of the solvent from the total absorbance of the sample. For QDs deposits on glass, we also measure their absorbance in transmission (normal incidence). A first reference measurement is made of the substrate alone (glass slide of the same thickness). The spectra of

QDs are therefore obtained by subtracting the absorbance of the glass substrate from the total absorbance of the sample.

X-ray Photoelectron Spectroscopy (XPS)
XPS spectra were collected on a SPECS GmbH PHOIBOS 100-1D delay line detector photoelectron spectrometer, using a monochromated AlKα (hv = 1486.6 eV) radiation source having a 250W electron beam power.

Fluorescence spectroscopy and microscopy
The fluorescence spectra presented in Figure 3 of this manuscript are obtained using an IHR-320 spectrofluorometer (Horiba) coupled with an SR-830 lock-in amplifier (Stanford Research System).

The fluorescence microscopy images presented in Figure 5 are obtained using an inverted DMi8 microscope equipped with a 40x/0.6 NA objective (Leica) and piloted with Metamoroph software. The epifluorescence pathway is equipped with a solid state light engine (Lumecor), a set of filter cubes and a camera (Flash4.0LT, Hamamastu Photonics). We use a 482/18 nm bandpass filter for the excitation spectral selection and a 520/28 nm bandpass filter for the fluorescence emission (GFP-1828A set, Semrock). The size of the field of view is 333 µm. Images were analysed with ImageJ.

Time-resolved fluorescence spectro-microscopy
The time-resolved fluorescence decays presented in Figure 4 are obtained using a custom made time-resolved laser scanning TCSPC microscope described previously [55]. Briefly, the setup is based on a TE2000 microscope with a 60x, 1.2NA water immersion objective (Nikon). The TCSPC path is equipped with a 440 nm pulsed laser diode (PicoQuant) driven by a PDL800 driver (PicoQuant). The fluorescence is selected by a 520/28 nm bandpass filter before the MCP-PMT detector (Hamamatsu Photonics). A C1 scanning head (Nikon) probes a 100µm x100µm field of view. The PicoHarp300 TCSPC module (PicoQuant) collects all the signals and data are processed with the SymPhoTime 64 software (PicoQuant). The TCSPC fluorescence decay of all the pixels of the field of view was computed by the SymPhoTime64 software and the decays were fitted with an exponential fit function (IgorPro, tri-exponential).

Two-colour sum-frequency generation spectroscopy (2C-SFG)
SFG spectra were acquired thanks to a home-made setup described elsewhere [21]. Briefly, it is based on a pulsed IR laser source from HighQ laser (Nd:YVO4, 1064 nm, 7.5 ps) coupled to an acousto-optic modulator (62.5 MHz micropulse repetition rate, 2 µs train, 25 Hz macropulse repetition rate). After amplification, it pumps two optical parametric oscillators (OPO). The infrared OPO is tunable over the 2500-4000 cm^{-1} spectral range while the visible OPO is tunable between 440 and 710 nm. As illustrated in Figure 6 for vibrational SFG spectra, the tunable IR and the two fixed visible (520 and 488 nm wavelength, respectively) beams are then coherently mixed at the same point of the functionalized surface of the glass substrate. The polarisation scheme is [s:sp] for the SFG, Visible and IR beams, respectively. The SFG beam is collected by photomultipliers after spatial and spectral filtering through a monochromator. For the SFG spectra obtained in Figure 6c, the IR beam is set at a fixed energy corresponding to the CH_2 asymmetric stretching mode (2937 cm^{-1}) while the visible beam is tuned between 650 and 450 nm (from red to blue). The momentum conservation rules in nonlinear optics implies that the output SFG beam spans a wider angular range with respect to the sample surface normal than in the case of vibrational SFG spectra.

References

[1] N. Nath, A. Chilkoti, A Colorimetric Gold Nanoparticle Sensor To Interrogate Biomolecular Interactions in Real Time on a Surface, Anal. Chem. 74 (2002) 504–509.

[2] A.-L. Morel, S. Boujday, C. Méthivier, J.-M. Krafft, C.-M. Pradier, Biosensors Elaborated on Gold Nanoparticles, a PM- IRRAS Characterisation of the Ig G Binding Efficiceny, Talanta. 85 (2011) 35–42.

[3] S.A. Jadhav, Self-assembled monolayers (SAMs) of carboxylic acids: an overview, Cent. Eur. J. Chem. 9 (2011) 369–378.

[4] C.A. Schoenbaum, D.K. Schwartz, J.W. Medlin, Controlling the Surface Environment of Heterogeneous Catalysts Using Self- Assembled Monolayers, Acc. Chem. Res. 47 (2014) 1438–1445.

[5] M. Ben Haddada, J. Blanchard, S. Casale, J.-M. Krafft, A. Vallée, C. Méthivier, S. Boujday, Optimizing the Immobilization of Gold Nanoparticles on Functionalized Silicon Surfaces: Amine- vs Thiol- Terminated Silane, Gold Bull. 46 (2013) 335–341.

[6] A. Lundgren, M. Hulander, J. Brorsson, M. Hermansson, H. Elwing, O. Anderson, B. Liedberg, M. Berglin, Gold-Nanoparticle-Assisted Self-Assembly of Chemical Gradients with Tunable Sub-50 nm Molecular Domains, Part. Part. Syst. Charact. 31 (2014) 209–218.

[7] L. Dalstein, M. Ben Haddada, G. Barbillon, C. Humbert, A. Tadjeddine, S. Boujday, B. Busson, Revealing the Interplay between Adsorbed Molecular Layers and Gold Nanoparticles by Linear and Nonlinear Optical Properties, J. Phys. Chem. C. 119 (2015) 17146–17155.

[8] K.C. Grabar, R.G. Freeman, M.B. Hommer, M.J. Natan, Preparation and Characterization of Au Colloid Monolayers, Anal. Chem. 67 (1995) 735–743.

[9] C. Humbert, O. Pluchery, E. Lacaze, A. Tadjeddine, B. Busson, Optical spectroscopy of functionalized gold nanoparticles assemblies as a function of the surface coverage, Gold Bull. 46 (2013) 299–309.

[10] W. Khalid, M. El Helou, T. Murböck, Z. Yue, J.-M. Montenegro, K. Schubert, G. Göbel, F. Lisdat, G. Witte, W. J. Parak, Immobilization of Quantum Dots via Conjugated Self-Assembled Monolayers and Their Application as a Light-Controlled Sensor for the Detection of Hydrogen Peroxide, *ACS Nano* 5, 9870–9876 (2011)

[11] E. V. Shevchenko, D. V. Talapin, C. B. J. Murray, S. O'Brien, Structural characterization of self-assembled multifunctional binary nanoparticle superlattices, *J. Am. Chem. Soc.* 128, 3620 (2006)

[12] T. Brezesinski, M. Groenewolt, A. Gibaud, N. Pinna, Evaporation-Induced Self-Assembly (EISA) at Its Limit: Ultrathin, Crystalline Patterns by Templating of Micellar Monolayers, M. Antonietti and B. M. Smarsly, *Adv. Mater.* 18, 2260 (2006)

[13] T. B. Norsten, B. L. Frankamp, V. N. Rotello, Metal Directed Assembly of Terpyridine-Functionalized Gold Nanoparticles, *Nano Lett.* 12, 1345 (2002)

[14] W. Shenton, D. Pum, U. B. Sleytr, S. Mann, Synthesis of cadmium sulphide superlattices using self-assembled bacterial S-layers, *Nature* 389, 585 (1997)

[15] J. P. Hoogenboom, C. Retif, E. de Bres, M. V. de Boer, A. K. van Langen-Suurling, J. Romijn, A. van Blaaderen, Template-induced growth of close-packed and non-close-

packed colloidal crystals during solvent evaporation, *Nano Lett.* 4 205 (2004)

[16] Y. Justo, I. Moreels, K. Lambert, Z. Hens, Langmuir–Blodgett monolayers of colloidal lead chalcogenide quantum dots: morphology and photoluminescence, *Nanotechnology* 21, 295606 (2010)

[17] A. Ulman, Formation and Structure of Self- Assembled Monolayers, Chem. Rev. 96 (1996) 1533–1554.

[18] Z. Hjezi, Biocéramiques phosphocalciques fonctionnalisées: étude de la silanisation de surface, Université de Limoges, 2015.

[19] P.H. Mutin, G. Guerrero, A. Vioux, Hybrid materials from organophosphorus coupling molecules, J. Mater. Chem. 15 (2005) 3761–3768.

[20] D.L. Angst, G.W. Simmons, Moisture Absorption Characteristics of Organosiloxane Self-Assembled Monolayers, Langmuir. 7 (1991) 2236–2242.

[21] T. Noblet, L. Dreesen, S. Boujday, C. Méthivier, B. Busson, A. Tadjeddine, C. Humbert, Semiconductor quantum dots reveal dipolar coupling from exciton to ligand vibration, Commun. Chem. 1 (2018) 76. doi:10.1038/s42004-018-0079-y.

[22] J.B. Blanco-Canosa, M. Wu, K. Susumu, E. Petryayeva, T.L. Jennings, P.E. Dawson, W.R. Algar, I.L. Medintz, Recent progress in the bioconjugation of quantum dots, Coord. Chem. Rev. 263–264 (2014) 101–137.

[23] Z. Grabarek, J. Gergely, Zero-length crosslinking procedure with the use of active esters, Anal. Biochem. 185 (1990) 131–135.

[24] D. Sehgal, I.K. Vijay, A Method for the High Efficiency of Water- Soluble Carbodiimide-Mediated Amidation, Anal. Biochem. 218 (1994) 87–91.

[25] R. Bilan, F. Fleury, I. Nabiev, A. Sukhanova, Quantum dot surface chemistry and functionalization for cell targeting and imaging, Bioconjug. Chem. 26 (2015) 609–624.

[26] S.H. Behrens, D.G. Grier, The charge of glass and silica surfaces, J. Chem. Phys. 115 (2001) 6716.

[27] P.W. Atkins, Physical Chemistry, 5th ed., Oxford University Press, 1994.

[28] J. Hottechamps, T. Noblet, A. Brans, C. Humbert, L. Dreesen, How quantum dots aggregation enhances Förster Resonant Energy Transfer, *ChemPhysChem* 21, ? (2020) doi:10.1002/cphc.202000067

[29] A. Shavel, N. Gaponik, A. Eychmüller, Covalent Linking of CdTe Nanocrystals to Amino-Functionalized Surfaces, *ChemPhysChem* 6, 449 (2005)

[30] S. K. Mishra, D. Kumar, A. M. Biradar, Rajesh, Electrochemical impedance spectroscopy characterization of mercaptopropionic acid capped ZnS nanocrystal based bioelectrode for the detection of the cardiac biomarker—myoglobin, *Bioelectrochemistry* 88, 118 (2012)

[31] T. Noblet, L. Dreesen, J. Hottechamps, C. Humbert, A global method for handling fluorescence spectra at high concentration derived from the competition between emission and absorption of colloidal CdTe quantum dots, Phys. Chem. Chem. Phys. 19 (2017) 26559–26565

[32] L. Dreesen, C. Humbert, M. Celebi, J.J. Lemaire, A.A. Mani, P.A. Thiry, A. Peremans, Influence of the metal electronic properties on the sum-frequency generation spectra of dodecanethiol self-assembled monolayers on Pt (111), Ag (111) and Au (111) single crystals, Appl. Phys. B Lasers Opt. 74 (2002).

[33] M. Raab, J.C. Becca, J. Heo, C.-K. Lim, A. Baev, L. Jensen, P.N. Prasad, L. Velarde, Doubly resonant sum frequency spectroscopy of mixed photochromic isomers on surfaces reveals conformation-specific vibronic effects, J. Chem. Phys. 150 (2019) 114704.

[34] L. Dreesen, C. Humbert, Y. Sartenaer, Y. Caudano, C. Volcke, A.A. Mani, A. Peremans, P.A. Thiry, S. Hanique, J.-M. Frère, Electronic and Molecular Properties of an Adsorbed Protein Monolayer Probed by Two- Color Sum-Frequency Generation Spectroscopy, Langmuir. 20 (2004) 7201–7207.

[35] Y. Caudano, C. Silien, C. Humbert, L. Dreesen, A.A. Mani, A. Peremans, P.A. Thiry, Electron-phonon couplings at C_{60} interfaces: a case study by two-color, infrared-visible sum-frequency generation spectroscopy, J. Electron Spectrosc. Relat. Phenom. 129 (2003) 139–147.

[36] K.C. Chou, S. Westerberg, Y.R. Shen, P.N. Ross, G.A. Somorjai, Probing the charge-transfer state of CO on Pt(111) by two-dimensional infrared-visible sum frequency generation spectroscopy, Phys. Rev. B. 69 (2004) 153413

[37] D. Elsenbeck, S.K. Das, L. Velarde, Substrate influence on the interlayer electron-phonon couplings in fullerene films probed with doubly-resonant SFG spectroscopy, Phys. Chem. Chem. Phys. 19 (2017) 18519.

[38] B. Bozzini, L. D?Urzo, C. Mele, B. Busson, C. Humbert, A. Tadjeddine, Doubly Resonant Sum Frequency Generation Spectroscopy of Adsorbates at an Electrochemical Interface, J. Phys. Chem. C. 112 (2008) 11791–11795.

[39] L. Dalstein, A. Revel, C. Humbert, B. Busson, Nonlinear optical response of a gold surface in the visible range: A study by two-color sum-frequency generation spectroscopy. I. Experimental determination, J. Chem. Phys. 148 (2018) 134701.

[40] C. Humbert, A. Dahi, L. Dalstein, B. Busson, M. Lismont, P. Colson, L. Dreesen, Linear and nonlinear optical properties of functionalized CdSe quantum dots prepared by plasma sputtering and wet chemistry, Journal of Colloid and Interface Science. 445 (2015) 69–75.

[41] L. Dalstein, C. Humbert, M. Ben Haddada, S. Boujday, G. Barbillon, B. Busson, The Prevailing Role of Hotspots in

Plasmon-Enhanced Sum-Frequency Generation Spectroscopy, J. Phys. Chem. Lett. 10 (2019) 7706–7711.

[42] D. Lis, Y. Caudano, M. Henry, S. Demoustier?Champagne, E. Ferain, F. Cecchet, Selective Plasmonic Platforms Based on Nanopillars to Enhance Vibrational Sum- Frequency Generation Spectroscopy, Adv. Opt. Mater. 1 (2013) 244–255.

[43] X. Toledo-Fuentes, D. Lis, F. Cecchet, Structural Changes to Lipid Bilayers and Their Surrounding Water upon Interaction with Functionalized Gold Nanoparticles, J. Phys. Chem. C. 120 (2016) 21399–21409.

[44] C. Humbert, T. Noblet, L. Dalstein, B. Busson, G. Barbillon, Sum- Frequency Generation Spectroscopy of Plasmonic Nanomaterials: A Review, Materials (Basel). 12 (2019) 836.

[45] O. Pluchery, C. Humbert, M. Valamanesh, E. Lacaze, B. Busson, Enhanced Detection of Thiophenol adsorbed on Gold Nanoparticles by SFG and DFG Nonlinear Spectroscopy, Phys. Chem. Chem. Phys. 11 (2009), 7729-7737.

[46] B. Busson, L. Dalstein, Sum-Frequency Spectroscopy Amplified by Plasmonics: The Small Particle Case, J. Phys. Chem. C. 123 (2019) 26597–26607.

[47] M. Linke, M. Hille, M. Lackner, L. Schumacher, S. Schlücker, E. Hasselbrink, Plasmonic Effects of Au Nanoparticles on the Vibrational Sum Frequency Spectrum of 4-Nitrothiophenol, J. Phys. Chem. C. 123 (2019) 24234–24242.

[48] R.M. Pasternack, A.S. Rivillon, Y.J. Chabal, Attachment of 3-(Aminopropyl)triethoxysilane on Silicon Oxide Surfaces: Dependence on Solution Temperature, Langmuir. 24 (2008) 12963–12971.

[49] J. Kim, G.J. Holinga, G.A. Somorjai, Curing Induced Structural Reorganization and Enhanced Reactivity of Amino- Terminated Organic Thin Films on Solid Substrates: Observations of Two Types of Chemically and Structurally Unique Amino Groups on the Su, Langmuir. 27 (2011) 5171–5175.

[50] M. Zhu, M.Z. Lerum, W. Chen, How To Prepare Reproducible, Homogeneous, and Hydrolytically Stable Aminosilane-Derived Layers on Silica, Langmuir. 28 (2012) 416–423.

[51] P.J.N. Kett, M.T.L. Casford, A.Y. Yang, T.J. Lane, M.S. Johal, P.B. Davies, Structural Changes in a Polyelectrolyte Multilayer Assembly Investigated by Reflection Absorption Infrared Spectroscopy and Sum Frequency Generation Spectroscopy, J. Phys. Chem. B. 113 (2009) 1559–1568.

[52] L.T. Zhuravlev, Concentration of Hydroxyl Groups on the Surface of Amorphous Silicas, Langmuir. 3 (1987) 316–318.

[53] L.T. Zhuravlev, The surface chemistry of amorphous silica, Colloids Surfaces A. 173 (2000) 1–38.

[54] S. Guhathakurta, A. Subramanian, Effect of Hydrofluoric Acid in Oxidizing Acid Mixtures on the Hydroxylation of Silicon Surface, J. Electrochem. Soc. 154 (2007) 136–146.

[55] M. Erard, A. Fredj, H. Pasquier, D.-B. Beltolngar, Y. Bousmah, V. Derrien, P. Vincent, F. Merola, Minimum set of mutations needed to optimize cyan fluorescent proteins for live cell imaging, Mol. BioSyst. 9 (2013) 258-267.